Experimental GNSS tomography study in Lisbon (Portugal)

PEDRO BENEVIDES, JOÃO CATALÃO, PEDRO MIRANDA
Instituto Dom Luíz (IDL), University of Lisbon, pjbenevides@fc.ul.pt

Recibido: 01/07/2014
Aceptado: 26/09/2014

Abstract
Water vapour variability on the atmosphere plays a crucial role on its dynamic processes, being difficult to quantify. The GNSS atmospheric processing has been developed in the past years providing integrated water vapour estimates. These integrated profiles lack a vertical discretization of the atmospheric processes. Reconstruction of the slant path observation in the satellite line of view allows to study the troposphere heterogeneity. 3D tomographic software was developed to model the troposphere dynamics throughout these GPS measurements. A GNSS network available in an area of 60 km^2 in Lisbon (Portugal) composed by 9 receivers was used for the software testing, and preliminary 4D tomography solutions were obtained. Radiosonde measurements were compared to validate the tomographic inversion solution. This study aims for a preliminary characterization of the 3D water vapour field over this region, which will help to assist the investigation of severe weather episodes.
Key words: GNSS meteorology, GNSS tomography, water vapour, precipitable water vapour, Lisbon.

Estudio experimental de tomografía GNSS en Lisboa (Portugal)

Resumen
La variabilidad de vapor de agua en la atmósfera juega un papel crucial en sus procesos dinámicos, siendo difícil de cuantificar. El proceso atmosférico GNSS se ha desarrollado en los últimos años proporcionando estimaciones de vapor de agua integrado. Estos perfiles integrados carecen de una discretización vertical de los procesos atmosféricos. La reconstrucción de la observación en la línea de vista del satélite permite estudiar la heterogeneidad de la troposfera. Se ha desarrollado un software para modelar la dinámica de la troposfera mediante medidas GPS. Se utilizó una red GNSS disponible en una zona de 60 km^2 en Lisboa (Portugal) compuesta por 9 receptores para el chequeo de software y se obtuvieron soluciones preliminares de tomografía 4D. Se compararon con mediciones de radiosonda para validar la solución. Este estudio tiene como objetivo la caracterización preliminar del campo de vapor de agua en esta región que ayudará en la investigación de episodios meteorológicos severos.
Palabras clave: Meteorología y tomografía GNSS, vapor de agua, vapor de agua precipitable, Lisboa.

Normalized reference
Benevides, P., Catalão, J., Miranda, P. (2014). Experimental GNSS tomography study in Lisbon (Portugal). *Física de la Tierra*, Vol. 26, 65-79.

Introduction

Water vapour variability on the atmosphere plays a crucial role on its dynamic processes, being difficult to quantify. Its high variability in the atmospheric processes triggers the moisture motions transport on a wide range of scales in space and time, influencing the evolution of meteorological phenomena and the current

weather state. The GNSS techniques, in particular the GPS has proved its capacity for sensing the water vapour variability, providing measurements of integrated water vapour (IWV) along a column of atmosphere above a station with the same accuracy as other classical meteorological observation methods like radiosonde, radiometer, lidar or radar (Bevis et al., 1992; Tregoning et al., 1998; Champollion et al., 2009). At present, the capability of the GNSS technique to estimate the total column of water vapour from a common receiver is widely accepted for meteorological studies (Lutz et al., 2010; Manning et al., 2012) and usually estimated in GPS routine analyses, more recently together with its horizontal gradients of tropospheric path delay to account for its isotropic variations, along with the equation solving residual observables containing small atmospheric contributions (Hirahara, 2000; Champollion et al., 2009; Bender et al., 2011; Van Baelen et al., 2011).

In the GPS processing software the integrated tropospheric wet delay value on the zenith is determined (Bevis et al., 1992; Flores et al., 2000). This integrated profile relates to a measurement of the total amount of water vapour but lacks a vertical discretization of the atmospheric processes, not allowing to identify where the water vapour is located in its tropospheric profile (Bastin et al., 2007; Bender et al., 2011). Taking advantage from the continuously growing GNSS station availability, processing the data from local and dense networks increases the number of information traveling the local troposphere and provides an opportunity for estimating the total amount of water vapour related to the refractivity in space and its temporal behaviour. (Gradinarsky et al., 2002; Bastin et al., 2007; Bender et al., 2011). The inverse theory of reconstruction of a 3D image from ray path integrated values, defining tomography, is based on the applications already used for health purposes in the medicine field and for Earth interior seismic reconstruction studies on geophysics field (Gradinarsky et al., 2002; Champollion et al., 2005; Rohm and Bosy, 2009). The GNSS tomographic formulation can successfully be applied to the local refractivity distribution in the troposphere above a dense network of stations (Hirahara, 2000; Champollion et al., 2005), providing 3D information about the state of the atmosphere at a current period, especially in resolving the vertical distribution of the water vapour (Flores et al., 2000; Troller et al., 2006).

Several campaigns and studies in the past years have already proven that tomography can yield a good spatial and temporal representation of the troposphere horizontal and vertical structures, providing better information for quantifying atmospheric phenomena (Flores et al., 2000; Hirahara, 2000; Champollion et al., 2005; Troller et al., 2006; Bastin et al., 2007; Champollion et al., 2009). Other measuring sensors like radiosondes provide a punctual sounding of the atmosphere, representing very local meteorological magnitudes (Flores et al., 2001), and opposite to the GNSS tomography that is capable of sensing its state globally and continuously throughout the signals crossing the atmosphere (Flores et al., 2000). Although the GNSS tomographic technique has limitations, especially the necessity of a dense distribution of stations to provide a large set of observations in a con-

fined area to avoid a negative impact of the noising in the solution reconstruction of the water vapour images (Champollion et al., 2005; Bender et al., 2011; Rohm, 2013; Shangguan et al., 2013).

A GNSS permanent network was available over an area of 60 km^2 in Lisbon (Portugal) composed by 9 receivers collecting data continuously. 3D tomographic GNSS software was developed to model the troposphere dynamics throughout the GPS measurements of slant path wet delay (SWD). One radiosonde station within the area is also available in order to validate the tomographic inversion solution. This study aims for a preliminary characterization of the 4D water vapour field over this region, leading to further future investigation of meteorological phenomenon.

1. Tomography

1.1 GNSS Tomography formulation

To retrieve the 3D water vapour density structure, a discretization of the troposphere on the study area has to be performed, where it is spatially divided into a finite number of boxes or cells (usually called voxels (Flores et al., 2000)) where it is assumed a constant value inside each (Flores et al., 2000; Troller et al., 2006; Bender et al., 2011). The grid model itself is represented by an arbitrary number of cells that is dependent from its horizontal and vertical geometrical resolution (Hirahara, 2000; Troller et al., 2002). During a desirable time period, each pair of station receiver and satellite generates an equation for each single instant, based on the reconstructed GNSS original slant ray path, which travels a distance inside each cell (Hirahara, 2000; Flores et al., 2000; Gradinarsky et al., 2002). Thus, through the application of mapping functions to reconstruct the slant path wet delay observation and partially model its ray bending, the latter can be negligible (Flores et al., 2001) reducing the system of equations problem to a geometrical linear approach (Champollion et al., 2005). A diagram of this procedure is reproduced in Figure 1.

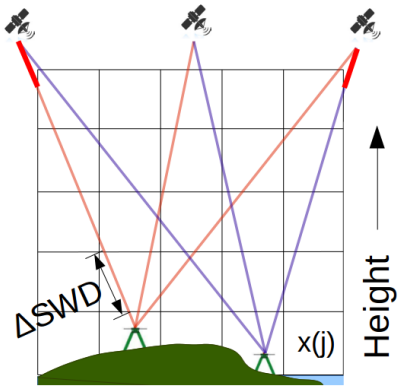

Fig. 1. Schematic representation of a 3D GNSS tomographic grid. 2 GPS stations ray tracing 3 satellites. Red bold lines represent SWD rays exiting the grid model laterally.

Delimiting the troposphere above an area with several receivers into cells and assuming a constant value, results in a discretization of the space model (Flores et al., 2000). Then the integral slant path of the GNSS wet delay can be expressed by the summation of *j* cells along the slant ray path (Hirahara, 2000; Flores et al., 2001). The length of each sub path traversing each cell (Fig. 1) can be represented on a design matrix *A*, that can be related to each unknown wet refractivity cell represented by a vector *x* and the slant wet path delay observable *y* or L_{SWD}, following the equation model in the form (Flores et al., 2000; Flores et al., 2001):

$$L_{SWD} = 10^{-6} \int_{s.p.} N_w \cdot ds \equiv L_{SWD}(i) = \sum_j a(i,j).x(j) \equiv y = Ax \qquad (1)$$

The matrix coefficients *a(i,j)* are the subsections of the *i* slant path distance in the *j* grid cell. The vector *x* represents the unknowns for each constant wet refractivity N_w value to be determined. The refractivity retrieved throughout the troposphere medium is mainly influenced by the water vapour density variability (Flores et al., 2000; Van Baelen et al., 2011). This system of equations represents a particular inverse problem where the main challenge is the inversion of the design matrix *A*. This matrix represents a linear operator that connects the slant path observations providing the length distribution of SWD through to the model parameters, forming a linear combination of the grid cells unknowns (Flores et al., 2000; Bastin et al., 2007; Van Baelen et al., 2011; Rohm, 2013). The estimation of the unknown water vapour content is obtained with the matrix inversion operation throughout the defined grid and hence this can be done by solving the linear system of equations throughout a least-squares approach (Troller et al., 2002; Rohm and Bosy, 2011). The limited geometry of the GNSS observations will not fully populate the grid resolution, hence resulting in several cells not crossed or intersected by any observation (Bender and Raabe, 2007). Therefore without initial conditions or additional constraints, the problem becomes locally undetermined (Flores et al., 2000; Troller et al., 2006; Champollion et al., 2005), resulting in an ill-conditioned or ill-posed problem (Gradinarsky et al.; Rohm and Bosy, 2009; Bender et al., 2011).

To solve the former the discrete inverse theory formulation is usually employed, based on a usual damped least squares method popular in seismic tomography that minimises equation 1 (left) (Menke, 2012). Hirahara (2000) adds horizontal and vertical constraints into the system of equations. Flores et al. (2000) uses a similar technique but on the inversion applies the singular value decomposition (SVD) and Kalman filtering. This filter allows to adapt the system sensibility to slow or rapid spatial variations on the water vapour state (Champollion et al., 2009). Other authors developed similar software with slightly different approaches, but in general following the above formulation (Troller et al., 2002; Champollion et al., 2005; Rohm and Bosy 2009; Notarpietro et al. 2011; Perler et al., 2011). Other methodologies for surpassing this issue were applied with success, using interactive alge-

braic reconstruction techniques, being particularly useful for resolving large number of data input and extensive grid cell configuration (Bender et al., 2011).

1.2 GPS framework

In order to retrieve the slant path wet delay input observations for the tomography model, a GPS data processing has to be performed. In this work scope the data was processed using GAMIT\GLOBK software (v10.5) (Herring et al., 2010) in daily double-difference sessions, tightly constraining the stations to the ITRF08 reference frame, adding several International GNSS Service (IGS) stations and using IGS precise final orbits. A second step is performed only running GAMIT with a set of configurations oriented on the enhancement of the atmospheric parameters, fixing the precise coordinates estimated in the first step and applying a time overlap window strategy (Haase et al., 2003) of 4 processing sessions of 12 hours each day, extracting the middle 6 hours. The final parameter obtained is defined as Zenith Total Delay (ZTD) and results from the sum of the two integral components, Zenith Hydrostatic Delay (ZHD) and Zenith Wet Delay (ZWD). ZTD is determined through a mean of all sets of slant path observations of delay from each station to all observed satellites in its horizon at a single instant. Thus it represents a volume on the troposphere resembling a cone extent (Champollion et al., 2005; Benevides et al., 2013) and is calculated using the aforementioned mapping functions. A 7º cut-off was fixed together with the VMF1 mapping functions (Boehm et al., 2006). ZTD is parameterized as a stochastic function variation of the ZHD using Gauss-Markov process with a power density function interpolated between temporal nodes. For this work ZTD are generated each 15 minute. ZHD is usually calculated with precision from climatological data or precise surface pressure measurements and is subtracted from the ZTD obtained from the solving of the GPS normal equations, and then ultimately the ZWD is calculated (Tregoning and Herring, 2006). For more information on the GPS processing issues one should consult Benevides et al. (2013). The time varying atmospheric characteristics observed from each ground-based GPS receiver can be transformed through a linear empirical relationship implying only an integrated weighted mean temperature of the atmosphere (*Tm*); Precipitable Water Vapour (PWV). Following Bevis et al. (1992), ZWD delays are converted in PWV using a constant factor κ depending on water vapour empirical constants and on *Tm*:

$$IWV = PWV = \kappa(Tm).ZWD \tag{2}$$

Tm was estimated for the Lisbon region climate as a linear function of the surface temperature through parameters calibrated with yearly series of radiosondes observations. PWV can be expressed in mm or equivalent kg/m^2 more commonly associated with the IWV nomenclature (Brenot et al., 2014), and represents the measurement of water if all of its columnar content would condensate. Wherefore it represents the total quantity of water vapour above a station expressed as the height

of an equivalent column of liquid water (Tregoning et al., 1998). Slant integrated water vapour (SIWV) can be estimated with the same methodology applied to the transition of the ZWD to PWV (Champollion et al., 2005).

2. Tomography preliminary results

In this experiment a GNSS permanent network was available over an area of 60 km^2 within Lisbon and around its vicinity, composed by 9 receivers with a regional distribution that can be observed on Figure 2. The location of the regional radiosonde station, near Lisbon centre, can also be observed. The digital terrain model shows the elevations with a crescent value proportional to a brighter tone, where the lower station (PACO) has 75 m and the higher station (ARRA) 409 m, representing a terrain with some plain and mountain areas, not being totally flat and hence suitable for GNSS tomographic inversion solutions (Flores et al., 2000, Champollion et al., 2005; Van Baelen et al., 2011).

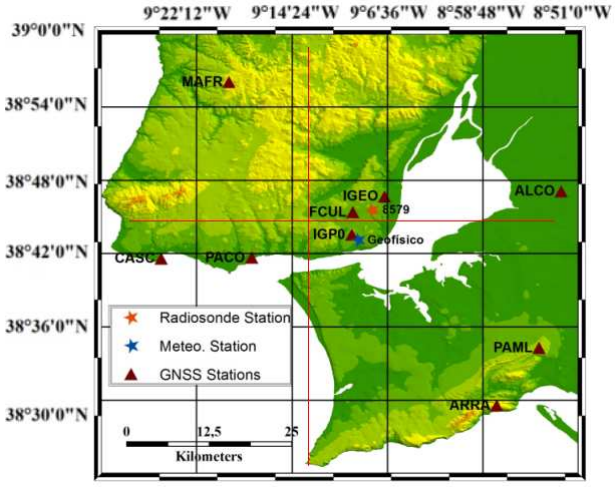

Fig. 2. Location of the GNSS network, meteorological and radiosonde stations in the study area, along with the 2D definition of the tomographic grid; 5 cells in longitudinal and 6 on latitudinal direction. Red lines represent the vertical cross section profiles of Figure 3.

A 3D geometrical grid was adjusted to the area in order to run tests over the tomographic GNSS developed software. The GNSS geometrical configuration chosen here is composed by a horizontal grid resolution of 5 cells on longitudinal direction and 6 on the latitudinal direction (Fig. 2). The mean station distance is found to be 45.5 km, which is 4 times larger than the approximated 11 km^2 grid size, although almost all stations being situated near the cell limit in order to more easily cover the vicinity grid cells with observations, minimizing empty voxels. The vertical grid is

composed by a variable sectioning of 18 layers with the bottom starting at 500 m altitude with a thinner separation of 250 m on the lower tropospheric region up to 2 km, increasing to 300 m up to 3 km, to 500 m up to 4 km, and having a regular 1 km separation above this and until the top boundary layer of 10 km. A thinner separation on the lower troposphere levels is desirable to model the water vapour dynamics since the majority of the tropospheric water vapour is present here. Horizontal and vertical grid resolution was empirically adjusted in order to obtain a feasible solution throughout the inversion of the implement system.

Slant path wet delay observations are retrieved for the ZWD GAMIT determination, using the mapping function formulation (Boehm et al., 2006) implemented in our software. At the 30 second GPS frequency rate, a SWD for each GPS station and satellite is determined from an interpolated value of the ZWD parameter, gathering a strong number observations rate. Since the tomography technique is highly sensible to small variations on the input data, for this preliminary study in order to avoid the possibility of the solution being affected by extra noise artefacts, the SWD are not converted into integrated SIWV measurements. Thus if one follows equation 2 for this conversion it may induct even more assumptions to the troposphere state since a mean temperature profile is used. Therefore SWD are introduced directly as input observations in mm units. Neither GPS residuals nor atmospheric gradients were introduced in the slant delay observations. Slant rays that cross the lateral boundaries of the defined grid are considered but constrained with a proportion given by the height of the vertical layer where the ray traverses the grid frontier. Following Perler et al. 2011, an exponential negative function is applied to the ratio between the height of the ray at the exiting layer and a scale factor that was adjusted to be 2200 m, similar to a standard atmosphere profile (Van Baelen et al., 2011). The remaining slant rays are indirectly constrained through the assumption that on the top vertical layer the water vapour content is none. The time interval for obtaining a water vapour map is defined to be 30 minutes, which is a reasonable period where a high variation on the weather state is not expected and a large amount of SWD observations can be collected.

Starting from the discrete inverse problem set by equation 1 (right) the damped least square formulation for the GNSS tomography problem is implemented here through the following system of equations:

$$x = (A^T.P.A)^{-1}.(A^T.P.y) \tag{3}$$

where y is the SWD observations, x the refractivity or the water vapour field solution and P is the observations weighted matrix. To overcome the geometrical limitation of the several empty cells that creates the ill-posed problem we add to the A matrix a spatial smoothing horizontal constraint that reflects a weighted average value of the cells vicinity. The weight was defined by the inverse distance of all the vicinity cells in the same layer. Fixation of the top vertical boundary layer with a null value is performed adding the constraint information in a similar way, and as in

the previous constraint zero values are added to the *y* vector. The ZWD mean profiles are introduced also in the tomographic equation system as external information with a discretization on the *A* matrix assuming the same negative exponential decay with altitude used for the characterization of the exiting rays that cross the grid lateral boundaries. The corresponding observation vector is fulfilled throughout a spatial interpolation of the ZWD station values filling horizontal cells without information, and each column of the grid model is equally scaled in altitude through the previous defined negative exponential function. The SWD observations weight represented by the diagonal elements of the *P* matrix are calculated with a 50% ponderation between the original ZWD estimated error in the GPS processing and the satellite elevation dependent error which is used to model the station error on GAMIT projecting the error along the ray path direction. A global parameter weight is given to each one of the constraints by adjusting empirically the values and comparing the obtained solution to a radiosonde available profile, which will be shown below. For the top zero value constraint the weight is unitary, contrasting with the down-weighted horizontal mean constraint by a 0.25 factor and the ZWD input constraint that was adjusted to a 0.29 value.

Observing the geometrical grid configuration, the temporal window for collecting observations and the constraints added, the characterization of the tomographic system in equation 4 is given by a number of unknown values 5x6x18 (540) and a set of 4000 to 5000 SWD input observations that generates the same amount of equations. Furthermore, the number of additional equations dependent of the horizontal constraints is equal to the total number of cells, and the equations related to the vertical and external constraints are equal each to one more layer of cells (30).

On Figure 3 are presented a set of profile examples of the tomography reconstruction for a late September 2012 intense precipitation episode. The first and third plot represent a West to East cross section profile and a South to North cross section profile respectively in the grid data (Figure 2 red lines) at the 12h of day 22, where a mean PWV value of 25 mm was observed and a relatively stable weather is reproduced by the tomography values. Gradual increment of the GPS signal led the PWV to rise about 20 mm in only 12 hours culminating with intense rainfall at the 2h of day 23. The second and fourth graphs on Figure 3 report the tomography retrieved for this date where it is noticed a high increment of the water vapour content in all the layers up to 3 km through all of its geographical extension. High temperature observed in this case may have driven the warm and humid air mass up in the troposphere provoking strong precipitation with saturation of the water vapour. Several hours after the storm the PWV values decrease to about 15 mm and low refractivity values on the 3D tomographic map are also noticed (not shown).

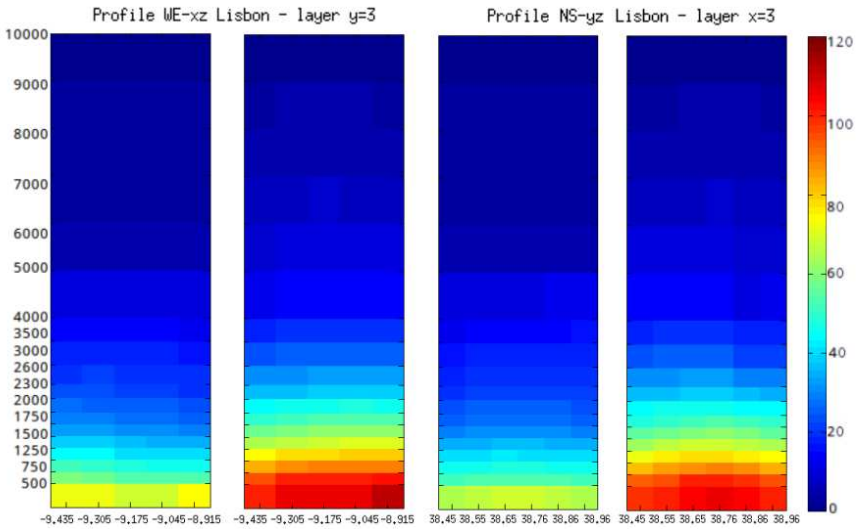

Fig. 3. West to east tomographic cross section profile for the 12h of 22/09/12 and 2h of 23/09/12, on the left, and the respective South to North profiles on the right. Values are in refractivity units (mm/km).

Radiosonde profiles launch near the Lisbon airport are used to validate our water vapour field reconstruction with independent measurements. This is done taking the columnar values of all the voxels in the correspondent vertical profile that match the horizontal grid position in which the launching station is located (Fig. 2). Values of temperature, pressure and relative humidity and some atmospheric constants related to Thayer (1974) refractivity formulation are used from the radiosonde data to calculate in each pressure layer a estimative comparable to the tomography.

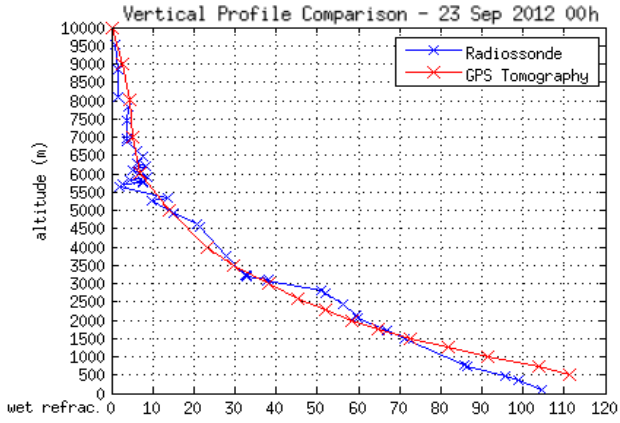

Fig. 4. Radiosonde and tomography (x=3, y=3) profiles comparison for the 0h day 23/09/12, with values in refractivity units (mm/km).

Hence, a comparison profile example can be considered in Figure 4 where a radiosonde profile launch at 0h of day 23 September 2012 is compared with the correspondent tomography solution column (x=3,y=3). Withal it is seen that the tomography has overestimated values on the lower levels until 1250 m, and further ahead from 5000 m to the top. Above 5000 m higher variations on radiosonde data with oscillations drawing larger spikes are not represented by the tomography. Due to water vapour high variability mainly in the lower levels, large deviations are expected (Champollion et al., 2009). Although generally the tomography values follow quite well the decrease revealed by the radiosonde throughout the height increment in the troposphere domain. When comparing the tomography approximated vertical profile that encompasses the radiosonde launch profile location one should notice that the latter measurements are instantaneous and punctual over a mean half hour that the sensor takes to reach about 10 km high. Withal radiosonde is affect by the wind, deflecting the vertical ascension unpredictably (Champollion et al., 2005). Moreover, we are comparing a vertical punctual profile with a mean columnar value from an 11 km^2 cell determined by the tomography. Therefore, these characteristics have to be taken into account in a comparison between these two techniques, especially when the troposphere is under strong atmospheric perturbations (Shangguan et al., 2013).

GNSS tomographic solutions are affected by a series of limitations derived from the technique, which have to be carefully considered in the analysis. Special care has to be taken in the global weight given to each constraint, particularly on the horizontal mean overweight which may smooth out variations in the solution (Troller et al., 2002), or in the underweight which will result in false spatial variations caused by the ill-posed condition. A better agreement between the GNSS tomography solution is usually obtained if the radiosonde profiles are assimilated as external input to the system (Champollion et al., 2005), providing an accurate vertical structure (Van Baelen et al., 2011). However in this experiment the goal was to evaluate the GPS capability to reproduce the water vapour variations alone, without additional independent meteorological information. Other fact that limits substantially the vertical resolution is the sparser distribution of the GPS stations causing a not optimal geometrical coverage on the grid cells (Bastin et al., 2007). Moreover the input SWD observations have a higher inaccuracy (Champollion et al., 2009) despite the different weight given depending on the elevation angle. Rohm (2012) quantified the SWD uncertainty applying the variance propagation law and estimated them varying from 10 to 50 mm depending on the elevation angle.

A last example of the tomography in the Lisbon region is introduced in Figure 5, where it is presented for a 3 day period from 30 August to 1 September 2011 a PWV evolution for the IGP0 station along with the hourly rainfall registered in the Geofísico station (Fig. 2), at the top, compared with the same tomography vertical profile used for radiosonde comparison which covers the locations of the previous stations, at the bottom. Analysing the PWV alone one can notice a strong 20 mm

increment on the first day, and a similar increment registered on the second day but here with presence of precipitation. Observing the vertical extra distribution information of the water vapour densities provided by the tomography it is shown on the second day, specifically on the hours prior to the intense rain (20h day 31 and 00h day 1) that the water vapour is more concentrated on the lower layers of the domain up to 1500 m, comparing with the peak registered on day 30. Moreover, a more pronounced and unstable water vapour behaviour seems to be registered on the day where the precipitation occurs. Reconstruction quality map seems affect by noisier signal above the 5 km altitude, despite these magnitude values being relative small compared with the tropospheric content on the grid lower layers.

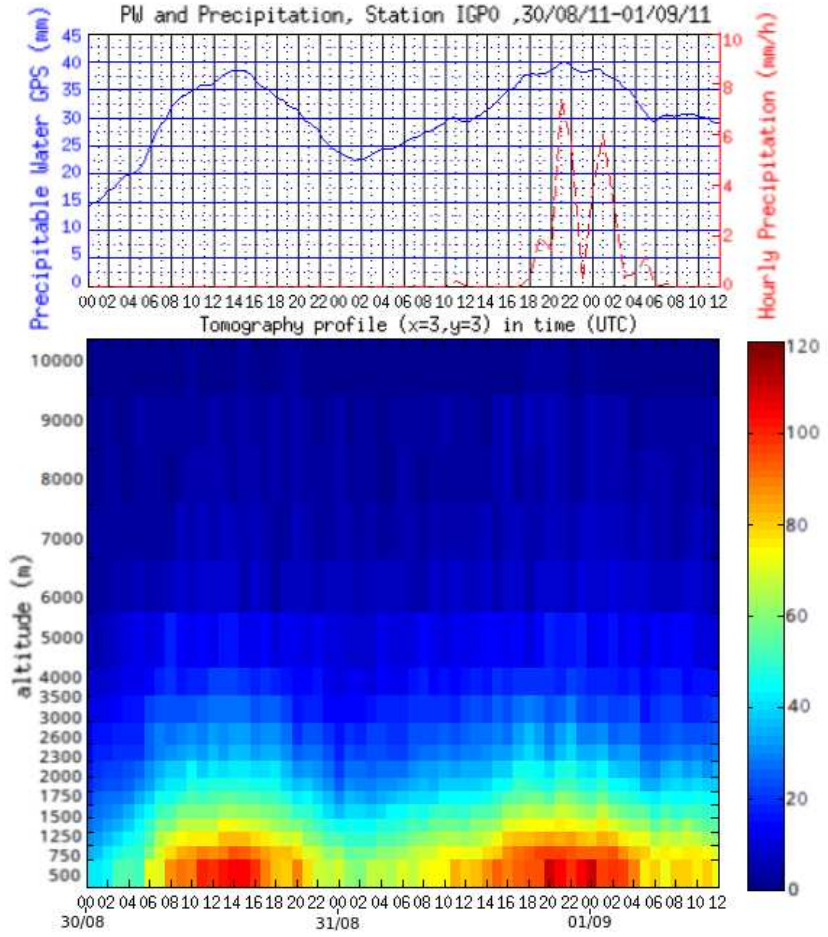

Fig. 5. PWV time plot for the IGP0 station compared with precipitation in Lisbon centre meteorological station (top). Tomography hourly profiles for the Lisbon centre (x=3, y=3) in the same time window (bottom), with values in refractivity units (mm/km).

3. Conclusion and Future work

The GNSS tomography technique application to the small scale station network available in the region of Lisbon was achieved successfully being determined a set of 4D preliminary maps that can describe water vapour variability. Vertical cross section profiles are retrieved with significant tropospheric wet refractivity characterization, and comparison with radiosonde profiles showed good agreement between the vertical distributions. Vertical transport of water vapour into close to saturation height above the PBL is evidenced. It is verified by the 4D temporal evolution of a tomography profile that the water vapour density increases mainly in the lower layers in the hours prior to an intense rain event. Hence our approach can provide unique high resolution additional spatial and temporal information, representing an unprecedented opportunity for a deepen study of severe weather episodes. The main drawback of the technique is the geometrical limitation of the SWD observations coverage creating an ill-posed formulation to the system solvability. Consequently, imposition of constraints and internal parameters calibration are necessary for the atmospheric reconstructions, which may induce errors on the water vapour characterization. Additional information is also vital for a meaningful tropospheric reconstruction especially in the vertical direction. Nevertheless the results on this paper show a feasible characterization of the tropospheric water vapour content mainly up to 5 km altitude.

A relevant number of future tasks can be approached for the enhancing of the GNSS tomography results. Implementing a Kalman filter in the time domain between consecutive map solutions can improve the precision of the inversion and smooth its sharper temporal variations (Hirahara, 2000; Champollion et al., 2005). Further tests are necessary to analyse the inclusion of the GPS residuals and gradient components in the tomography since their impact on the solution is not clear to benefit the solution or overcharge it with additional error (Flores et al., 2000; Champollion et al., 2005; Brenot et al., 2014) Comparison with 2D PWV interpolated maps are a good example for inspecting the lateral water vapour anomalies retrieval from the introduction of these residual quantities in the observations. Densification of GNSS stations on a region, throughout the planning of a field campaign with temporarily installed receivers (Champollion et al., 2005) increases the number of information traveling the local troposphere and thus the geometrical coverage of the grid domain (Flores et al., 2001), providing a better resolution and precision on the 4D tomographic maps. Additional GNSS observations to the system input should also bring benefits through a new set of observations in a different view than the GPS satellites, such as the actual GLONASS and the future Galileo (Champollion et al., 2005; Bender et al., 2011). The assimilation of external meteorological measurements to the system resolution, likewise ground based radiometers, LIDAR, solar spectrometers, or remote sensing radio occultation should improve the GNSS tomography accuracy results (Champollion et al., 2009; Notarpietro et al., 2011). Assimilation of the GPS data products in numerical

weather prediction models (NWP) can benefit its forecasting capability (Flores et al., 2001), especially in the additional information of water vapour vertical distribution provided by the GNSS tomography (Lutz et al., 2010), and in the direct assimilation of SWD data providing information on the anisotropy of current state of the troposphere (Bastin et al., 2007). If tomography is available in near real time it is also a valid method for a quantitative analysis of the NWP high resolution forecast results (Champollion et al., 2005; Lutz et al., 2010). Moreover, the wet refractivity field maps from the tomography can be applied in the compensation of atmospheric features present on several remote sensing data such as InSAR or MODIS sensor images.

Acknowledgements
Fundação para a Ciência e Tecnologia (FCT), for the PhD grant SFRH/BD/80288/2011.

References

BASTIN, S., CHAMPOLLION, C., BOCK, O., DROBINSKI, P., & MASSON, F. (2007). Diurnal cycle of water vapor as documented by a dense GPS network in a coastal area during ESCOMPTE IOP2. *Journal of applied meteorology and climatology*, 46(2), 167-182.

BENDER, M., & RAABE, A. (2007). Preconditions to ground based GPS water vapour tomography. *Annales Geophysicae*, Vol. 25, No. 8, pp. 1727-1734.

BENDER, M., DICK, G., GE, M., DENG, Z., WICKERT, J., KAHLE, H.-G., RAABE, A. and TETZLAFF, G. (2011). Development of a GNSS water vapour tomography system using algebraic reconstruction techniques. *Advances in Space Research*, 47, 10, 1704-1720, doi:10.1016/j.asr.2010.05.034

BENEVIDES, P., CATALÃO, J., MIRANDA, P., & CHINITA, M. J. (2013). Analysis of the relation between GPS tropospheric delay and intense precipitation. *SPIE Remote Sensing* (pp. 88900Y-88900Y). International Society for Optics and Photonics.

BEVIS, M., BUSINGER, S., HERRING, T., ROCKEN, C., ANTHES, R. A. AND WARE R.H., (1992). GPS meteorology: remote sensing of the atmospheric water vapor using the Global Positioning System, *Journal of Geophysical Research*, 97, No. D14, October 20 1992, pp. 15787–15801, doi:10.1029/92JD01517

BOEHM, J., WERL, B. AND SCHUH, H., (2006). Troposphere mapping functions for GPS and very long baseline interferometry from European Centre for Medium-Range Weather Forecasts operational analysis data, *Journal of Geophysical Research*, 111, p. B02406, doi:10.1029/2005JB003629

BRENOT, H., WALPERSDORF, A., REVERDY, M., VAN BAELEN, J., DUCROCQ, V., CHAMPOLLION, C., ... & GIROUX, P. (2014). A GPS network for tropospheric tomography in the framework of the Mediterranean hydrometeorological observatory Cévennes-Vivarais (southeastern France). *Atmospheric Measurement Techniques*, 7(2), 553-578.

CHAMPOLLION, C., MASSON, F., BOUIN, M. N., WALPERSDORF, A., DOERFLINGER, E., BOCK, O., & VAN BAELEN, J. (2005). GPS water vapour tomography: preliminary results from the ESCOMPTE field experiment. *Atmospheric research*, 74(1), 253-274.

CHAMPOLLION, C., FLAMANT, C., BOCK O., MASSON, F., TURNER, D. D. AND WECKWERTH, T. (2009). Mesoscale GPS tomography applied to the 12 June 2002 convective initiation event of IHOP 2002, *Quarterly Journal of the Royal Meteorological Society*, 135, Issue 640, pages 645–662, April 2009 Part A, doi:0.1002/qj.386

FLORES, A., RUFFINI, G., & RIUS, A. (2000). 4D tropospheric tomography using GPS slant wet delays. *Annales Geophysicae*, Vol. 18, No. 2, pp. 223-234.

FLORES, A., DE ARELLANO, J. G., GRADINARSKY, L. P., & RIUS, A. (2001). Tomography of the lower troposphere using a small dense network of GPS receivers. *Geoscience and Remote Sensing*, IEEE Transactions on, 39(2), 439-447.

GRADINARSKY, L., JARLEMARK, P., & JOHANSSON, J. (2002). GPS tomography using the permanent network in Goteborg: simulations. *Position Location and Navigation Symposium*, 2002 IEEE (pp. 128-133). IEEE.

HAASE, J., GE, M., VEDEL, H. AND CALAIS, E., (2003). Accuracy and Variability of GPS Tropospheric Delay Measurements of Water Vapor in the Western Mediterranean, *Journal of Applied Meteorology*, 42 (11), pp.1547-1568

HERRING, T., KING, R. W. AND MCCLUSKY, S. C., (2010). GAMIT Reference Manual – GPS Analysis at MIT – Release 10.4, Dep. of Earth, Atm. and Planetary Sciences, MIT.

HIRAHARA, K. (2000). Local GPS tropospheric tomography. *Earth, planets and space*, 52(11), 935-939.

LUTZ, S., TROLLER, M., PERLER, D., GEIGER, A., & KAHLE, H. G. (2010). Better weather prediction using GPS. *GPS World*, 21(7), 40-47.

MANNING, T., ZHANG, K., ROHM, W., CHOY, S., & HURTER, F. (2012). Detecting severe weather using GPS tomography: an Australian case study. *J. of Glob. Pos. Sys*, 11(1), 58-70.

MENKE, W. (2012). Geophysical data analysis: discrete inverse theory. Academic press.

NOTARPIETRO, R., CUCCA, M., GABELLA, M., VENUTI, G., & PERONA, G. (2011). Tomographic reconstruction of wet and total refractivity fields from GNSS receiver networks. *Advances in Space Research*, 47(5), 898-912.

PERLER, D., GEIGER, A., & HURTER, F. (2011). 4D GPS water vapor tomography: new parameterized approaches. *Journal of Geodesy*, 85(8), 539-550.

ROHM, W., & BOSY, J. (2009). Local tomography troposphere model over mountains area. *Atmospheric Research*, 93(4), 777-783.

ROHM, W., & BOSY, J. (2011). The verification of GNSS tropospheric tomography model in a mountainous area. *Advances in Space Research*, 47(10), 1721-1730.

ROHM, W. (2012). The precision of humidity in GNSS tomography. Atmospheric research, 107, 69-75.

ROHM, W. (2013). The ground GNSS tomography–unconstrained approach. *Advances in Space Research*, 51(3), 501-513.

SHANGGUAN, M., BENDER, M., RAMATSCHI, M., DICK, G., WICKERT, J., RAABE, A., & GALAS, R. (2013). GPS tomography: validation of reconstructed 3-D humidity fields with radiosonde profiles. *Annales Geophysicae*, Vol. 31, No. 9, pp. 1491-1505. Copernicus GmbH.

THAYER, G. D. (1974). An improved equation for the radio refractive index of air. *Radio Science*, 9(10), 803-807.

TREGONING, P., BOERS, R., O'BRIEN, D., & HENDY, M. (1998). Accuracy of absolute precipitable water vapor estimates from GPS observations. *Journal of Geophysical Research: Atmospheres* (1984–2012), 103(D22), 28701-28710.

TREGONING, P. AND HERRING, T., (2006) Impact of a priori zenith hydrostatic delay errors on GPS estimates of station heights and zenith total delays, *Geophysical Research Letters*, 33, L23303, doi:10.1029/2006GL027706

TROLLER, M., BÜRKI, B., COCARD, M., GEIGER, A., & KAHLE, H. G. (2002). 3-D refractivity field from GPS double difference tomography. *Geophysical research letters*, 29(24), 2-1.

TROLLER, M., GEIGER, A., BROCKMANN, E., BETTEMS, J. M., BÜRKI, B., & KAHLE, H. G. (2006). Tomographic determination of the spatial distribution of water vapor using GPS observations. *Advances in Space Research*, 37(12), 2211-2217.

VAN BAELEN, J., REVERDY, M., TRIDON, F., LABBOUZ, L., DICK, G., BENDER, M., & HAGEN, M. (2011). On the relationship between water vapour field evolution and the life cycle of precipitation systems. *Quarterly Journal of the Royal Meteorological Society*, 137(S1), 204-223.